

# Ion sieving in graphene oxide membranes via cationic control of interlayer spacing

Liang Chen<sup>1,2,3\*</sup>, Guosheng Shi<sup>2\*</sup>, Jie Shen<sup>4\*</sup>, Bingquan Peng<sup>1\*</sup>, Bowu Zhang<sup>2</sup>, Yuzhu Wang<sup>2</sup>, Fenggang Bian<sup>2</sup>, Jiajun Wang<sup>1</sup>, Deyuan Li<sup>1,2</sup>, Zhe Qian<sup>1</sup>, Gang Xu<sup>1</sup>, Gongping Liu<sup>4</sup>, Jianrong Zeng<sup>2</sup>, Lijuan Zhang<sup>2</sup>, Yizhou Yang<sup>2</sup>, Guoquan Zhou<sup>3</sup>, Minghong Wu<sup>1</sup>, Wanqin Jin<sup>4</sup>, Jingye Li<sup>2</sup> & Haiping Fang<sup>2</sup>

Graphene oxide membranes—partially oxidized, stacked sheets of graphene<sup>1</sup>—can provide ultrathin, high-flux and energy-efficient membranes for precise ionic and molecular sieving in aqueous solution<sup>2–6</sup>. These materials have shown potential in a variety of applications, including water desalination and purification<sup>7–9</sup>, gas and ion separation<sup>10–13</sup>, biosensors<sup>14</sup>, proton conductors<sup>15</sup>, lithium-based batteries<sup>16</sup> and super-capacitors<sup>17</sup>. Unlike the pores of carbon nanotube membranes, which have fixed sizes<sup>18–20</sup>, the pores of graphene oxide membranes—that is, the interlayer spacing between graphene oxide sheets (a sheet is a single flake inside the membrane)—are of variable size. Furthermore, it is difficult to reduce the interlayer spacing sufficiently to exclude small ions and to maintain this spacing against the tendency of graphene oxide membranes to swell when immersed in aqueous solution<sup>21–25</sup>. These challenges hinder the potential ion filtration applications of graphene oxide membranes. Here we demonstrate cationic control of the interlayer spacing of graphene oxide membranes with ångström precision using  $K^+$ ,  $Na^+$ ,  $Ca^{2+}$ ,  $Li^+$  or  $Mg^{2+}$  ions. Moreover, membrane spacings controlled by one type of cation can

efficiently and selectively exclude other cations that have larger hydrated volumes. First-principles calculations and ultraviolet absorption spectroscopy reveal that the location of the most stable cation adsorption is where oxide groups and aromatic rings coexist. Previous density functional theory computations show that other cations ( $Fe^{2+}$ ,  $Co^{2+}$ ,  $Cu^{2+}$ ,  $Cd^{2+}$ ,  $Cr^{2+}$  and  $Pb^{2+}$ ) should have a much stronger cation– $\pi$  interaction with the graphene sheet than  $Na^+$  has<sup>26</sup>, suggesting that other ions could be used to produce a wider range of interlayer spacings.

There have been previous efforts to tune the interlayer spacing. For example, it can be widened, to increase the permeability of the graphene oxide membrane (GOM), by intercalating large nanomaterials<sup>21,22</sup> as well as by cross-linking large and rigid molecules<sup>23</sup>. Reducing GOMs can lead to a sharp decrease in the interlayer spacing, but renders them highly impermeable to all gases, liquids and aggressive chemicals<sup>24,25</sup>. Recent work reported a way of sieving ions through GOMs by encapsulating the graphene oxide sheets in epoxy films and varying the relative humidity<sup>27</sup> to tune the interlayer spacing. It remains difficult to reduce the interlayer spacing sufficiently (to less than a nanometre) to exclude

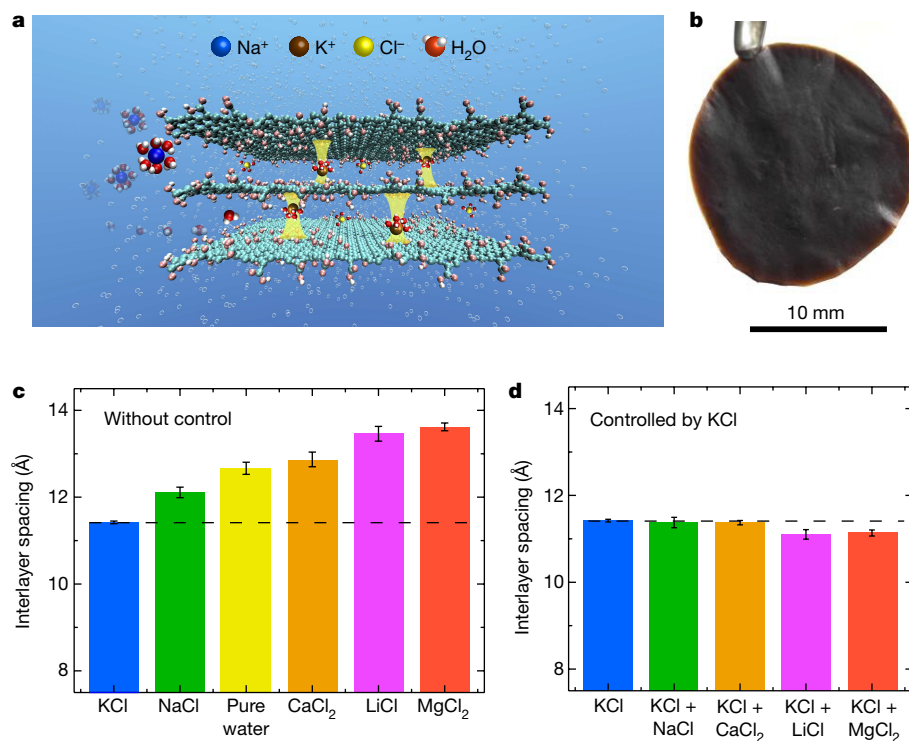


**Figure 1 | Interlayer spacings in freestanding cation-controlled GOMs.** **a**, A schematic of how  $K^+$  ions in a GOM determine and fix the interlayer spacing such that other cations are rejected while pure water can penetrate. Yellow pillars between the graphene oxide sheets depict the fixation of interlayer spacing by hydrated  $K^+$ . **b**, Photograph of a freestanding GOM prepared by drop-casting of a  $5 \text{ mg ml}^{-1}$  graphene oxide suspension. **c**, Interlayer spacings for GOMs immersed in pure water or in various  $0.25 \text{ mol l}^{-1}$  ( $0.25 \text{ M}$ ) salt solutions. **d**, Interlayer spacings of GOMs that were soaked in KCl solution, followed by immersion in various salt solutions. Error bars indicate the standard deviation from three different points of a sample.

<sup>1</sup>Shanghai Applied Radiation Institute, Shanghai University, Shanghai 200444, China. <sup>2</sup>Division of Interfacial Water, Key Laboratory of Interfacial Physics and Technology and Shanghai Synchrotron Radiation Facility, Shanghai Institute of Applied Physics, Chinese Academy of Sciences, Shanghai 201800, China. <sup>3</sup>Zhejiang Provincial Key Laboratory of Chemical Utilization of Forestry Biomass, Zhejiang A&F University, Lin'an, Zhejiang 311300, China. <sup>4</sup>State Key Laboratory of Materials-Oriented Chemical Engineering, Jiangsu National Synergetic Innovation Center for Advanced Materials, Nanjing Tech University, 5 Xinmofan Road, Nanjing 210009, China.

\*These authors contributed equally to this work.

small ions while still permitting water flow and enabling scalable production<sup>25</sup>. This limits the potential of GOMs for separating ions from bulk solution or for sieving ions of a specific size range from a mixed salt solution—such as the most common ions in sea water and those in the electrolytes of lithium-based batteries and super-capacitors ( $\text{Na}^+$ ,  $\text{Mg}^{2+}$ ,  $\text{Ca}^{2+}$ ,  $\text{K}^+$  and  $\text{Li}^+$ )<sup>2,25</sup>. Here we combine experimental observations and theoretical calculation to show that cations ( $\text{K}^+$ ,  $\text{Na}^+$ ,  $\text{Ca}^{2+}$ ,  $\text{Li}^+$  and  $\text{Mg}^{2+}$ ) themselves can determine and fix the interlayer spacing of GOMs at sizes as small as a nanometre and the variable range of this spacing can be controlled to within one ångström.

Freestanding GOMs were prepared from a graphene oxide suspension via the drop-casting method (see Supplementary Information section PS1). These GOMs were then immersed for one hour in 0.25 mol l<sup>-1</sup> (0.25 M) solutions of KCl, NaCl, CaCl<sub>2</sub>, LiCl and MgCl<sub>2</sub>. Next, the GOMs, now saturated with salt solution, were removed and analysed by X-ray diffraction. There were clear shifts of the interlayer spacing (indicated by the Bragg peaks in Supplementary Fig. 3A) relative to the GOMs that had been immersed in pure water. Immersion in pure water resulted in a GOM spacing of  $12.8 \pm 0.2$  Å, consistent with early reports<sup>2,23</sup>. For ionic solutions the spacings were  $11.4 \pm 0.1$  Å,  $12.1 \pm 0.2$  Å,  $12.9 \pm 0.2$  Å,  $13.5 \pm 0.2$  Å and  $13.6 \pm 0.1$  Å for KCl, NaCl, CaCl<sub>2</sub>, LiCl and MgCl<sub>2</sub> solutions, respectively (Fig. 1c). Thus, the order from widest to narrowest spacing was MgCl<sub>2</sub> > LiCl > CaCl<sub>2</sub> > pure water > NaCl > KCl. The interlayer spacing of 11.4 Å in KCl solution is even smaller than the narrowest previously reported interlayer spacing of GOMs in aqueous solution (about 13 Å)<sup>2,23,28</sup>. We confirmed these interlayer spacings using two-dimensional synchrotron wide-angle X-ray scattering patterns (details in Supplementary Information section PS3), which showed the same order of ion-controlled interlayer spacing as did our experimental X-ray diffraction results.

In addition, we analysed the solution adsorption of freestanding GOMs treated with different ions. The wet masses of the freestanding GOMs that had been immersed in the KCl, NaCl, CaCl<sub>2</sub>, LiCl and MgCl<sub>2</sub> solutions after removal of the solutions on the surface by centrifugation were 2.4, 3.6, 3.0, 3.6 and 3.1 times the dry masses of the corresponding pristine (that is, not immersed in solution) freestanding GOMs, respectively (Fig. 2a). There is no clear order for the wet masses for ions of different valences, which we attribute to the existence of ripples in the membranes, allowing different amounts of the salt solution to be adsorbed (details in Supplementary Information section PS3). Following treatment with NaCl, CaCl<sub>2</sub>, LiCl, and MgCl<sub>2</sub> solutions, the dry masses determined after drying the saturated membranes at 60 °C for 6 h were greater than those of the corresponding pristine dry membranes, indicating that the salts are retained within the GOMs to some extent.

However, the dry mass of the KCl-treated membrane was approximately equal to that of the pristine dry membrane (Fig. 2a). This indicates very little penetration of KCl into the GOMs, which was further confirmed by X-ray photoelectron spectroscopy (Supplementary Fig. 5). Thus, the GOM immersed in KCl solution rejects most of the  $\text{K}^+$  ions but still allowed water to penetrate the membrane.

Just one kind of cation can control the interlayer spacing, potentially excluding other cations that require a larger interlayer spacing. Since the KCl solution produced the narrowest interlayer spacing, we first soaked freestanding GOMs in pure water, and subsequently immersed them in KCl solution. We next added other ion solutions of the same concentration. For these mixed solutions, the X-ray diffraction spectra differed only slightly from the spectrum acquired with the pure KCl solution (Supplementary Fig. 3B). The corresponding interlayer spacings were  $11.4 \pm 0.2$  Å,  $11.4 \pm 0.1$  Å,  $11.2 \pm 0.2$  Å and  $11.2 \pm 0.1$  Å, respectively, for KCl + M, where M = NaCl, CaCl<sub>2</sub>, LiCl or MgCl<sub>2</sub> (Fig. 1d). Moreover, these interlayer spacings remained consistent over more than 140 h, indicating a stable saturation effect and equilibrium adsorption of cations (Supplementary Fig. 6A). These results clearly demonstrate that  $\text{K}^+$  stably and effectively fixed the interlayer spacing at about 11 Å, resulting in the rejection of other cations in mixed solutions

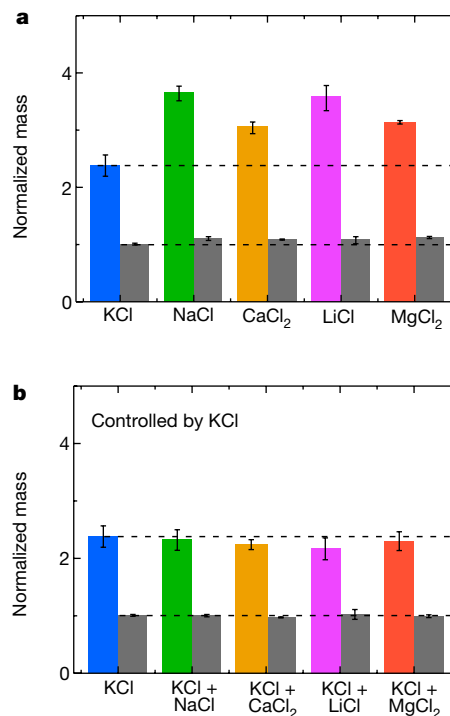
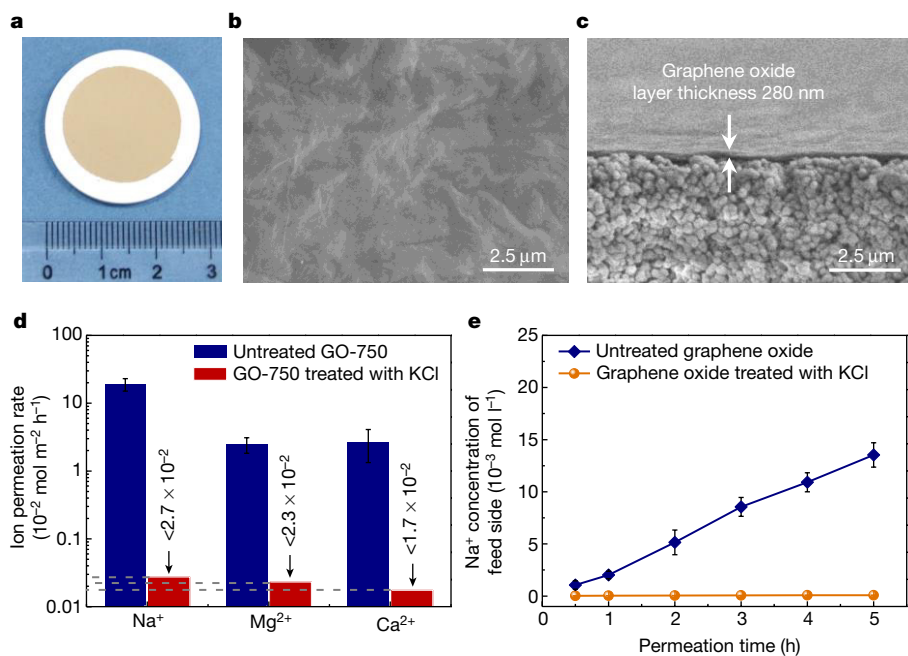


**Figure 2 | Solution adsorption of freestanding GOMs with different ions.** **a**, Wet and dry masses of freestanding GOMs after immersion in various salt solutions, normalized by the corresponding dry mass of a pristine GOM. Wet and dry masses were obtained after removal of the solution on the membrane surface by centrifugation followed by drying at 60 °C for 6 h. Two dashed lines correspond to the normalized dry mass of a pristine GOM, and the normalized wet mass of a KCl-treated membrane. **b**, Normalized wet and dry masses of GOMs that were first soaked in KCl solution, and then immersed in various salt solutions. The coloured bars represent the mass of wet GOMs containing salt solution; the black bars represent the mass of dry GOMs containing salt. Error bars indicate the standard deviation from three different samples.

(including  $\text{K}^+$  itself). We also tested the control of interlayer spacing using NaCl/CaCl<sub>2</sub>, finding that  $\text{Na}^+$  and  $\text{Ca}^{2+}$  also fixed the interlayer spacings and excluded other cations that required larger interlayer spacings (details in Supplementary Information section PS6).

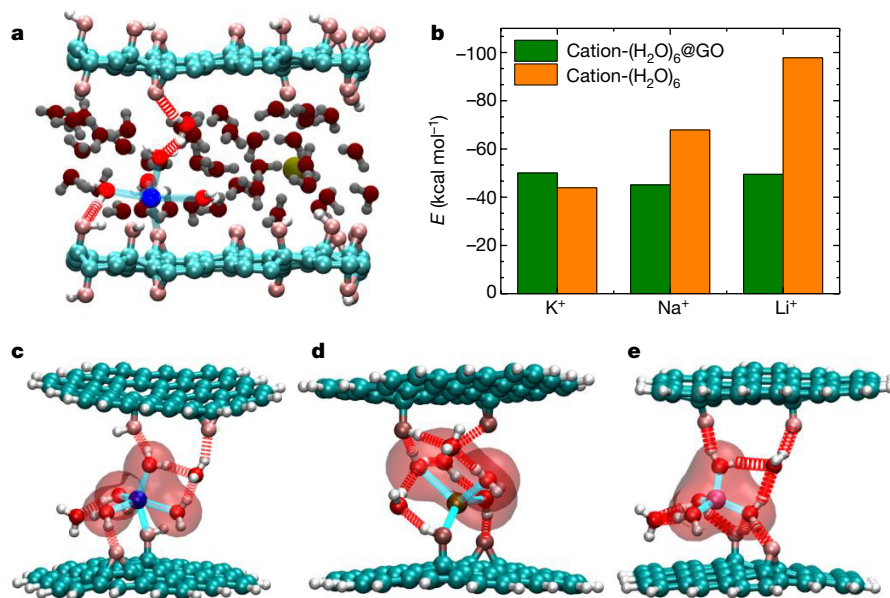
To further demonstrate the controlling effects of cations, we fabricated GOMs supported by ceramic substrates and used them for ion permeation tests. Graphene oxide layers were uniformly deposited on an Al<sub>2</sub>O<sub>3</sub> substrate (Fig. 3a). Scanning electron microscope images showed that the resulting thin layered membrane with tuneable thickness was continuous and free of macro pores or defects (Fig. 3b,c), which is critical for a highly efficient separation process<sup>6,29,30</sup>. We used GO-750 GOMs, which have a thickness of about 750 nm, in ion permeation tests (Fig. 3d). Untreated GO-750 GOMs showed  $\text{Na}^+$ ,  $\text{Mg}^{2+}$  and  $\text{Ca}^{2+}$  permeation rates of  $0.190 \text{ mol m}^{-2} \text{ h}^{-1}$ ,  $0.025 \text{ mol m}^{-2} \text{ h}^{-1}$  and  $0.019 \text{ mol m}^{-2} \text{ h}^{-1}$ , respectively. In contrast, KCl-treated GO-750 membranes showed low  $\text{Na}^+$ ,  $\text{Mg}^{2+}$  and  $\text{Ca}^{2+}$  permeation rates below the cation detection limits. This demonstrates the ion sieving effect of the KCl-controlled graphene oxide sheets, showing ion rejection of more than 99% relative to untreated GOMs. Here ion rejection refers to the reduction in ion permeation rate. Water could still pass through the KCl-controlled GO-750 membrane, showing a flux of about  $0.11 \text{ m}^{-2} \text{ h}^{-1}$  (Supplementary Table 2). Figure 3e shows that a thinner KCl-controlled GOM (GO-280) exhibited a higher water flux of  $0.361 \text{ m}^{-2} \text{ h}^{-1}$ , and still effectively rejected  $\text{Na}^+$ , with the permeation rate reduced by a factor of about 150 compared with the untreated GO-280 GOM. Additionally, mixed-ion permeation experiments (Supplementary Figs 9–11) revealed that KCl- and NaCl-controlled



membranes could efficiently reject ions even with a high salt concentration gradient. Importantly, we also observed rejection of  $\text{K}^+$  itself (Supplementary Fig. 11), consistent with the adsorption results. The order in which the graphene oxide is exposed to ions is important for efficient ion sieving. We further studied the effects of membrane thickness and salt concentration of the draw side solution (the draw side solution has a higher salt concentration than does the feed side solution, to generate the osmotic pressure gradient) (Supplementary Figs 12 and 13). Most GOMs can effectively sieve ions for about 5 h. Interestingly, when we used reduced GOMs (Supplementary Fig. 14),

the KCl-controlled reduced GOMs showed stable performance for over 24 h.

We further performed an *ab initio* molecular dynamics simulation to illustrate the underlying physical mechanism taking place in these membranes, using  $\text{Na}^+$  as an example. During the first 14 ps, the  $\text{Na}^+$  moves from between two graphene oxide sheets to a position near the bottom graphene oxide sheet (Supplementary Fig. 15), and then adsorbs at the regions where oxidized groups and aromatic rings coexist (Fig. 4a). Importantly, the lifetime of the hydrogen bonds belonging to the water molecules surrounding the  $\text{Na}^+$  ion and participating in



and graphene oxide sheets (labelled cation- $(\text{H}_2\text{O})_6$ @GO), and the hydration energy of the cation (labelled cation- $(\text{H}_2\text{O})_6$ ). **c–e**, The most stable optimized geometries of cation- $(\text{H}_2\text{O})_6$ @GO clusters from density functional theory computation, where the cations are  $\text{Na}^+$  (**c**),  $\text{K}^+$  (**d**) and  $\text{Li}^+$  (**e**). The transparent red area is the van der Waals volume of the hydration water molecules, showing that  $\text{K}^+$  has a larger volume (than the other two ions) when it is not surrounded by hydration water, and indicating a clear distortion of the hydrated structure of  $\text{K}^+$  inside the graphene oxide sheets.

and graphene oxide sheets (labelled cation- $(\text{H}_2\text{O})_6$ @GO), and the hydration energy of the cation (labelled cation- $(\text{H}_2\text{O})_6$ ). **c–e**, The most stable optimized geometries of cation- $(\text{H}_2\text{O})_6$ @GO clusters from density functional theory computation, where the cations are  $\text{Na}^+$  (**c**),  $\text{K}^+$  (**d**) and  $\text{Li}^+$  (**e**). The transparent red area is the van der Waals volume of the hydration water molecules, showing that  $\text{K}^+$  has a larger volume (than the other two ions) when it is not surrounded by hydration water, and indicating a clear distortion of the hydrated structure of  $\text{K}^+$  inside the graphene oxide sheets.

the connection with the oxygen functional groups in the two GOMs (highlighted in Fig. 4a) was approximately 30 times the lifetime of the hydrogen bond in pure water, indicating that hydrated  $\text{Na}^+$  binds the graphene oxide sheets through a stable hydrogen-bond network.

Density functional theory computation further confirmed that the most stable adsorption position for the cations  $\text{K}^+$ ,  $\text{Na}^+$  and  $\text{Li}^+$  was the region where oxidized groups and aromatic rings coexist (Fig. 4c–e). Molecular orbital analysis clearly revealed coupling between the lone pair of electrons of the oxygen atoms in the oxygen functional groups and the delocalized  $\pi$  states of the aromatic ring structure in graphene oxide and the empty orbitals of the cation (Supplementary Fig. 16B). This indicated that the fixing of the interlayer distances was mainly due to the interaction between the hydrated cations and aromatic rings (cation– $\pi$  interactions<sup>31</sup>) on the graphene oxide sheet, as well as the interaction between the hydrated cations and the oxidized groups on the graphene oxide sheet. The existence of these interactions has been confirmed by ultraviolet absorption spectral and X-ray absorption fine structure measurement experiments we performed (Supplementary Figs 17 and 18).

It was surprising that  $\text{K}^+$ -controlled GOMs rejected  $\text{K}^+$  itself. However, our computation revealed that, for  $\text{K}^+$  only, the interaction energy between the hydrated cation and graphene oxide sheets was comparable to the cation's hydration energy (Fig. 4b). This suggests that the  $\text{K}^+$  hydration structure is unstable when the hydrated  $\text{K}^+$  enters the space between graphene oxide sheets. Figure 4d shows a clear distortion of the hydrated structure of  $\text{K}^+$  inside the graphene oxide sheets, narrowing the interlayer spacing. This makes it difficult for other hydrated  $\text{K}^+$  ions to enter the space between graphene oxide sheets.

In summary, we have experimentally achieved facile and precise control of the interlayer spacing in GOMs, with a precision of down to 1 Å, and corresponding ion rejection, through the addition of one kind of cation. This method is based on our understanding of the strong noncovalent hydrated cation– $\pi$  interactions between hydrated cations and the aromatic ring, and its production is scalable. We note that our previous density functional theory computations show that other cations ( $\text{Fe}^{2+}$ ,  $\text{Co}^{2+}$ ,  $\text{Cu}^{2+}$ ,  $\text{Cd}^{2+}$ ,  $\text{Cr}^{2+}$  and  $\text{Pb}^{2+}$ ) have a much stronger cation– $\pi$  interaction with the graphene sheet<sup>26</sup>, suggesting that other ions could be used to produce a wider range of interlayer spacings. Overall, our findings represent a step towards graphene-oxide-based applications, such as water desalination and gas purification, solvent dehydration, lithium-based batteries and supercapacitors and molecular sieving.

**Data Availability** All data generated or analysed during this study are included in this Letter (and its Supplementary Information).

**Received 16 August 2016; accepted 15 August 2017.**

**Published online 9 October 2017.**

- Dikin, D. A. *et al.* Preparation and characterization of graphene oxide paper. *Nature* **448**, 457–460 (2007).
- Joshi, R. K. *et al.* Precise and ultrafast molecular sieving through graphene oxide membranes. *Science* **343**, 752–754 (2014).
- Elimelech, M. & Phillip, W. A. The future of seawater desalination: energy, technology, and the environment. *Science* **333**, 712–717 (2011).
- Gin, D. L. & Noble, R. D. Designing the next generation of chemical separation membranes. *Science* **332**, 674–676 (2011).
- Han, Y., Xu, Z. & Gao, C. Ultrathin graphene nanofiltration membrane for water purification. *Adv. Funct. Mater.* **23**, 3693–3700 (2013).
- Liu, G. P., Jin, W. Q. & Xu, N. P. Graphene-based membranes. *Chem. Soc. Rev.* **44**, 5016–5030 (2015).
- Sun, P. *et al.* Selective trans-membrane transport of alkali and alkaline earth cations through graphene oxide membranes based on cation– $\pi$  interactions. *ACS Nano* **8**, 850–859 (2014).
- Surwade, S. P. *et al.* Water desalination using nanoporous single-layer graphene. *Nat. Nanotechnol.* **10**, 459–464 (2015).
- Lin, L. C. & Grossman, J. C. Atomistic understandings of reduced graphene oxide as an ultrathin-film nanoporous membrane for separations. *Nat. Commun.* **6**, 8335 (2015).
- Celebi, K. *et al.* Ultimate permeation across atomically thin porous graphene. *Science* **344**, 289–292 (2014).

- Kim, H. W. *et al.* Selective gas transport through few-layered graphene and graphene oxide membranes. *Science* **342**, 91–95 (2013).
- Li, H. *et al.* Ultrathin, molecular-sieving graphene oxide membranes for selective hydrogen separation. *Science* **342**, 95–98 (2013).
- Koenig, S. P., Wang, L., Pellegrino, J. & Bunch, J. S. Selective molecular sieving through porous graphene. *Nat. Nanotechnol.* **7**, 728–732 (2012).
- Liu, Y. X., Dong, X. C. & Chen, P. Biological and chemical sensors based on graphene materials. *Chem. Soc. Rev.* **41**, 2283–2307 (2012).
- Lozada-Hidalgo, M. *et al.* Sieving hydrogen isotopes through two-dimensional crystals. *Science* **351**, 68–70 (2016).
- Yao, F. *et al.* Diffusion mechanism of lithium ion through basal plane of layered graphene. *J. Am. Chem. Soc.* **134**, 8646–8654 (2012).
- Wang, H. L. *et al.* Graphene-wrapped sulfur particles as a rechargeable lithium-sulfur battery cathode material with high capacity and cycling stability. *Nano Lett.* **11**, 2644–2647 (2011).
- De Volder, M. F. L., Tawfik, S. H., Baughman, R. H. & Hart, A. J. Carbon nanotubes: present and future commercial applications. *Science* **339**, 535–539 (2013).
- Koga, K., Gao, G. T., Tanaka, H. & Zeng, X. C. Formation of ordered ice nanotubes inside carbon nanotubes. *Nature* **412**, 802–805 (2001).
- Liu, J., Shi, G. S., Guo, P., Yang, J. R. & Fang, H. P. Blockage of water flow in carbon nanotubes by ions due to interactions between cations and aromatic rings. *Phys. Rev. Lett.* **115**, 164502 (2015).
- Huang, H. B. *et al.* Ultrafast viscous water flow through nanostrand-channelled graphene oxide membranes. *Nat. Commun.* **4**, 2979 (2013).
- Goh, K. *et al.* All-carbon nanoarchitectures as high-performance separation membranes with superior stability. *Adv. Funct. Mater.* **25**, 7348–7359 (2015).
- Hung, W. S. *et al.* Cross-linking with diamine monomers to prepare composite graphene oxide-framework membranes with varying d-spacing. *Chem. Mater.* **26**, 2983–2990 (2014).
- Su, Y. *et al.* Impermeable barrier films and protective coatings based on reduced graphene oxide. *Nat. Commun.* **5**, 4843 (2014).
- Sun, P., Wang, K. & Zhu, H. Recent developments in graphene-based membranes: structure, mass-transport mechanism and potential applications. *Adv. Mater.* **28**, 2287–2310 (2016).
- Shi, G. S. *et al.* Ion enrichment on the hydrophobic carbon-based surface in aqueous salt solutions due to cation– $\pi$  interactions. *Sci. Rep.* **3**, 3436 (2013).
- Abraham, J. *et al.* Tunable sieving of ions using graphene oxide membranes. *Nat. Nanotechnol.* **12**, 546–550 (2017).
- Raidongia, K. & Huang, J. Nanofluidic ion transport through reconstructed layered materials. *J. Am. Chem. Soc.* **134**, 16528–16531 (2012).
- Shen, J. *et al.* Membranes with fast and selective gas-transport channels of laminar graphene oxide for efficient  $\text{CO}_2$  capture. *Angew. Chem. Int. Ed.* **54**, 578–582 (2015).
- Huang, K. *et al.* A graphene oxide membrane with highly selective molecular separation of aqueous organic solution. *Angew. Chem. Int. Ed.* **53**, 6929–6932 (2014).
- Mahadevi, A. S. & Sastry, G. N. Cation– $\pi$  interaction: its role and relevance in chemistry, biology, and material science. *Chem. Rev.* **113**, 2100–2138 (2013).

**Supplementary Information** is available in the online version of the paper.

**Acknowledgements** We thank P. Ball, L. Kong, J. Liu, Z. Hou, G. Lei and H. Yang for constructive suggestions. We acknowledge support from the National Natural Science Foundation of China (grant numbers 11290164, 41430644, 21490585, 11574339, 11404361 and 21476107), the National Science Fund for Outstanding Young Scholars (number 11722548), the Key Research Program of the Chinese Academy of Sciences (grant number KJZD-EW-M03), the Deepcomp7000 and ScGrid of the Supercomputing Center, the Computer Network Information Center of the Chinese Academy of Sciences, the Special Program for Applied Research on SuperComputation of the NSFC-Guangdong Joint Fund (second phase), the Shanghai Supercomputer Center of China, and the BL16B1 and BL14W1 beamlines at the Shanghai Synchrotron Radiation Facility.

**Author Contributions** H.F. had the idea of controlling the interlayer spacing using ions based on cation– $\pi$  interactions. H.F., M.W., W.J., J.L. and G.S. designed the experiments and simulations. L.C., G.S., J.S., B.P., G.X., B.Z., Y.W., F.B., J.W., D.L., Z.Q., G.L., J.Z. and L.Z. performed the experiments. G.S., Y.Y. and L.C. performed the simulations. G.S., L.C., H.F., J.L., W.J., M.W., G.X. and G.Z. analysed the data, G.S., L.C., H.F., W.J. and M.W. co-wrote the paper. All authors discussed the results and commented on the manuscript.

**Author Information** Reprints and permissions information is available at [www.nature.com/reprints](http://www.nature.com/reprints). The authors declare no competing financial interests. Readers are welcome to comment on the online version of the paper. Publisher's note: Springer Nature remains neutral with regard to jurisdictional claims in published maps and institutional affiliations. Correspondence and requests for materials should be addressed to H.F. ([fanghaiping@sinap.ac.cn](mailto:fanghaiping@sinap.ac.cn)), M.W. ([mhwu@mail.shu.edu.cn](mailto:mhwu@mail.shu.edu.cn)), W.J. ([wqjin@njtech.edu.cn](mailto:wqjin@njtech.edu.cn)) or J.L. ([lijingye@sinap.ac.cn](mailto:lijingye@sinap.ac.cn)).

**Reviewer Information** *Nature* thanks R. Karnik and the other anonymous reviewer(s) for their contribution to the peer review of this work.